Published in final edited form as:

Inhal Toxicol. 2018 ; 30(11-12): 429–438. doi:10.1080/08958378.2018.1547334.

Modification of Nano-Silver Bioactivity by Adsorption on Carbon nanotubes and Graphene Oxide

Raymond F. Hamilton[1], **Zheqiong Wu**[2], **Megha Thakkar**[2], **Andrij Holian**[1], and **Somenath Mitra**[2]

[1]Center for Environmental Health Sciences, University of Montana, Missoula MT 59812, USA.

[2]Department of Chemistry and Environmental Science, New Jersey Institute of Technology, Newark, New Jersey 07102, USA.

Abstract

Objective: The toxicity of silver nanomaterials in various forms has been extensively evaluated, but the toxicity of silver nanocarbon composites is less well understood. Therefore, silver-carbon nanotube composites (Ag-MWCNT-COOH) and silver-graphene oxide composites (Ag-GO) were synthesized by microwave irradiation and evaluated in two *in vitro* cell models.

Materials/methods: Toxicity of silver nanosphere (Ag), Ag-MWCNT-COOH and Ag-GO were analyzed by MTS assay and LDH assay in primary C57BL/6 murine alveolar macrophages and human THP-1 cells. Activation of NLRP3 inflammasome by particle variants in these models was done by proxy using LPS co-culture and IL-1β release.

Results: The results depended on the model, as the amount of Ag on the modified carbon resulted in slightly increased toxicity for the murine cells, but did not appear to affect toxicity in the human cell model. IL-1β release from carbon particle-exposures was decreased by the presence of Ag in both cell models. Suspensions of Ag-MWCNT-COOH, Ag-GO and Ag in artificial lysosomal fluid were prepared and ICP-MS was used to detect Ag ions concentration in three silver suspension/solutions. The amount of Ag ions released from Ag-MWCNT-COOH and Ag-GO were similar, which were both lower than that of Ag nanospheres.

Conclusion: The results suggest the bioactivity of silver composites may be related to the amount of Ag ions released, which can be dependent on the cell model under investigation.

Keywords

macrophage; silver nanomaterials; MWCNT; NLRP3 inflammasome; silver ions

Introduction

Silver nanoparticles have found a wide range of applications as disinfecting agents based on their outstanding properties such as stability, durability, heat resistance, and broad spectrum

*Corresponding author: Andrij Holian (406-243-4018).

Disclosure Statement

The authors reported no potential conflict of interest.

antibacterial activity (Kim et al. 2007) (Chudasama et al. 2009). These applications include medical devices, home appliances to water treatment, food storage and textile coatings (Abou El-Nour et al. 2010). Silver nanomaterials have also been used in nanoscale sensors to increase response times and lower detection limits based on their electrochemical properties (Manno et al. 2008) and are used as biological tags for quantitative detection in numerous assays. Some chemical reactions such as reduction of 4-nitrophenol with $NaBH_4$ in alkaline aqueous solutions (Liu P and Zhao 2009), and chemiluminescence from luminol–hydrogen peroxide system (Guo et al. 2008) can be catalyzed by silver nanoparticles. In addition, optical properties of silver nanoparticles have led to their incorporation into optical spectroscopy for efficiently harvesting light (Rashid et al. 2013).

In general, many nanomaterials coexist with free ions or other soluble forms in their suspension. Some of these are oxides which undergo dissolution, such as ZnO and NiO (Martin et al. 2012) while others are zero-valent metal such as Au, which release ions by oxidative dissolution (Martin et al. 2012). The dissolution of Ag nanospheres contrasted with the dissolution of Ag on the carbon materials is a slightly different process, affecting kinetics, in the formation of Ag ions (Kittler et al. 2010; Liu JY and Hurt RH 2010). In addition, the release of ions, in general, from nanoparticles alters the properties of the nanomaterial suspensions, such as pH, temperature, toxicity and bioactivity (Maurer-Jones et al. 2013) (Chang et al. 2012). The toxicity of metal oxide nanomaterials, such as CuO and ZnO, to algae and aquatic invertebrates has been reported due to the formation of their soluble forms (Chang et al. 2012). It has been reported that 6-17% of silver in nanoparticle suspensions were in ionic forms which influenced changes in gene expression to silver nanoparticles (Bouwmeester et al. 2011). Therefore, it is important to study the effect of ionic species formation from new composite nanomaterials.

Typical silver nanoparticle suspensions are mixtures of silver ions, single nanoparticles, and aggregated nanoparticles (Hadrup and Lam 2014). Due to the large production volume, silver is released into environment in the form of silver ions, silver nanoparticles, and aggregations during usage and disposal, which may increase the risk for human health (Hussain and Schlager 2009) and environmental contamination (Liu J et al. 2010). It has been speculated that the biological effects of silver nanoparticles may originate from the reactive environment on their surface, their mechanical disruption of anatomical structures, and/or silver ions that are released from the surface of the particles (Hadrup and Lam 2014).

It is has been proposed that the toxicity of silver nanoparticles depends on the amount of silver ions released from the surface of the particles (Zhang et al. 2003; Lee et al. 2005; Morones et al. 2005; Choi and Hu 2008; He et al. 2013). The concentration of dissolved silver released from silver nanoparticle depends upon several factors such as surface area, oxidative dissolution of silver nanoparticles associated with supporting matrix, dissociation of dissolved silver and transport from the matrix, and adsorption equilibrium of dissolved silver onto supporting material (He et al. 2013; Hamilton et al. 2014). Ion release has been reported to be an oxidation process involving dissolved oxygen and proton concentration (Equation 1) (Liu J and Hurt RH 2010). Fuvlic acid was demonstrated to inhibit this reaction, the reason including surface adsorption to block silver nanoparticle oxidation sites and reversible reaction of released silver ion to silver as reductant (Liu J and Hurt RH 2010).

It has been reported that carbon can delay the release of silver ions from nanoparticles, but the mechanism is not well understood (He et al. 2013). In the carbon reducing environment, a possibility is that C=C groups may enhance the reduction of dissolved silver ions to silver nanoparticles (He et al. 2013). Therefore, it is important to investigate the effect of carbon as the supporting material on antibacterial ability of silver nanoparticles.

$$2\mathrm{Ag}_{(s)} + \frac{1}{2}\mathrm{O}_{2(aq)} + 2H^{+}_{(aq)} \leftrightarrow 2\mathrm{Ag}^{+}_{(aq)} + \mathrm{H}_2\mathrm{O}_{(1)} \quad (1)$$

The objective of this research is to determine if the toxicity of silver attached to CNT and GO would be reduced compared to pure Ag nanospheres, assuming the increased affinity of Ag to the carbon backbone would effectively decrease toxicity. All nanomaterials were characterized (e.g. size, solubility, zeta potential, endotoxin, etc…), including the release of Ag in simulated lysosomal fluid. The study also compared the toxicity of silver nanoparticles and silver composites. The toxicity and ability to activate the NLRP3 inflammasome of all the materials was evaluated using two models of macrophages.

Methods

Particles

Multiwall carbon nanotubes (MWCNT) (OD 20–30 nm, length 10–30 mm, purity >95%) were purchased from Cheap Tubes Inc., Graphene oxide (GO) (500 nm – 20 μm) was purchased from TW Nano Material Suppliers, and all other chemicals were purchased from Sigma Aldrich with purity higher than 95%.

Preparation of MWCNT-COOH

The synthesis of the carboxylated multiwall carbon nanotubes (MWCNT-COOH) was carried out under the Microwave Accelerated Reaction system by dispersing pre-weighed MWCNT into a mixture of concentrated H_2SO_4 and HNO_3. The reaction vessels were subject to microwave irradiation at 140°C for 20 min. After cooling down to room temperature, the product was vacuum filtered and washed using Milli-Q water through pore size 10 μm filter paper until a neutral pH was obtained. MWCNT-COOH samples were then dried in a vacuum oven at 70°C until a constant weight was achieved (Chen and Mitra 2008).

Preparation of Ag-MWCNT-COOH and Ag-GO

The MWCNT-COOH and graphene oxide was used to synthesize the Ag-MWCNT-COOH and Ag-GO hybrids. Typically, MWCNT-COOH aqueous solutions and $AgNO_3$ in ethylene glycol (EG) solutions were prepared prior to mixing. The mixture solutions were subject to microwave radiation at 100°C for 5 min. The product was filtered, washed with Milli-Q water until a neutral pH was obtained. Ag-MWCNT-COOH were obtained by drying at 50°C in a vacuum oven until constant weight. Ag-GO was prepared the same way as Ag-MWCNT-COOH.

Particle Characterizations

Scanning electron microscopy (SEM) data for samples were collected on a LEO 1530 VP scanning electron microscope. Elemental analysis was done using an energy-dispersive X-ray analyzer (EDX). Samples were characterized using transmission electron microscopy (TEM, Hitachi H-7500). Samples were dispersed in Milli-Q water, added to 200-mesh TEM grids and dried before operation. Thermo gravimetric analysis (TGA) was performed using a Pyris 1 TGA from Perkin–Elmer Inc. from 25°C to 800°C under a flow of air at 10 mL/min, at a heating rate of 10°C per min. Silver ion concentration released from Ag-MWCNT-COOH, Ag-GO and Ag nanospheres in artificial lysosomal fluid (ALF)(Marques et al. 2011) was quantified using Agilent 7500 ICP-MS. The same concentration of Ag-MWCNT-COOH, Ag-GO and Ag nanospheres in ALF solutions was prepared and mixed for 2 hours under 37°C. All samples were centrifuged prior to ICP-MS at 28,900 × *g* for 20 min to remove nanoparticles. All standards were prepared from a multi-element solution at 10 mg/L (Spex Certiprep) with addition of an internal standard mix (Li6, Ge, Y, In, Tb, Bi). ALF was added to all standards to match sample matrix. For calibration verification, multi-element instrument calibration standard 1, 20 mg/L (Spex Certiprep) was used. All samples were diluted 10x with water with addition of internal standard mix.

Particle size and zeta potential relevant to *in vitro* cell culture were measured in RPMI media (25 μg/mL) at 25°C using a Malvern Zetasizer nano Zen 3600 (Malvern Instruments, Worcestershire, UK) at a 90° detector angle (Table 1). Endotoxin contamination was determined by washing/sonicating 1 mg/mL MWCNT in endotoxin-free water for 30 min followed by centrifugation at 16,000 × *g* for 15 min prior to assay. The endotoxin assay (ToxinSensor) was performed on the isolated supernatant according to the manufacturer's protocol (GenScript, Piscataway, NJ). Aggregate size was expressed as nm ± the standard deviation. The zeta potential was expressed as mV ± the standard deviation. A list of particles, with regard to hydrodynamic size, zeta potential and endotoxin contamination, exclusively used in this study is shown in Table 2.

Preparation of the functionalized-MWCNT and Suspensions

All particle variants were weighed and suspended in dispersion media (DM) (Porter et al. 2008), which consisted of mouse serum albumin (Sigma, St. Louis, MO; 1 mg/mL) and 1,2 dipalmitoyl-sn-glycero-3-phosphocholine (DSPC, Sigma, 1 μg/mL) diluted in phosphate-buffered saline (PBS). Nanotube suspensions were sonicated for 5 min at 1/3 max power in a Qsonica cup-horn sonicator (Q500, Newtown, CT) attached to a circulating water-bath (VWR International, Radnor, PA) at 500 watts and 20 Hz (8000 Joules) at a stock concentration of 1 mg/mL.

Human THP-1 Cell Line Culturing

THP-1 cells, a human monocytic cell line obtained from ATCC, were suspended in RPMI media (MediaTech, Manassas, VA) supplemented with 10% fetal bovine serum, 50 μM beta-mercapto ethanol, 1 mM sodium pyruvate, 250 ng/mL amphotericin B, and 100 U/mL penicillin and streptomycin (all supplements Media Tech, Manassas, VA) in 75 cm^2 flasks at 37°C. The cells in suspension were differentiated into a macrophage-like cell by adding 150 nM Vitamin D_3 for 24 h. The resulting semi-adherent cells were scraped with a rubber

policeman in the existing media (Corning, Corning, NY). The cells were then centrifuged at 400 × *g* for 5 min, the resulting cell pellet was re-suspended in 1 mL of complete media, and a 40 μL sample was then counted on a Z2 Coulter Counter (Beckman Coulter, Miami, FL). The cells were suspended at 1×10^6 cells/mL and a small amount of phorbol 12-myristate 13-acetate (5 nM PMA, Sigma) and lipopolysacharride (10 ng/mL LPS, Sigma) was added. PMA co-stimulation was necessary to stimulate aggressive phagocytosis of the MWCNT. LPS co-stimulation was necessary to induce NF-κB activation, which leads to procaspase 1 formation, and in conjunction with particle-induced inflammasome activation, activated caspase-1 cleaves pro-IL-1β to IL-1β in the THP-1 model (Dostert et al. 2008; Palomaki et al. 2011). Cells, at a volume of 350 μL, were then pipetted into 1.5 mL microfuge tubes. The particle variants were used in a range of concentrations (0, 6.25, 12.5, 25, and 50 μg/mL). The resulting cell/particle suspension was mixed by pipette action. The cells were then transferred to 96-well tissue culture plates at 100 μL per well in triplicate (100×10^3 cells/well), and cultured for an additional 24 h. All cultures were maintained in 37°C water-jacketed CO_2 incubators (ThermoForma, Houston, TX). Viability and IL-1β levels were determined as described below. Three to four experimental replicates were done for each experiment.

Animals

C57Bl/6 (2-months old, male) were housed in controlled environmental conditions (22 ± 2°C; 30-40% humidity, 12-h light: 12-h dark cycle) and provided food and water *ad libitum*. All procedures were performed under protocols approved by the IACUC of the University of Montana.

Alveolar macrophage isolation: Mice were euthanized by sodium pentobarbital (Euthasol™ Schering-Plough, Lot# 1JRR11V), and the lungs with the heart were removed. Lung lavage was performed using ice-cold PBS (pH 7.4). Lung lavage cells were isolated by centrifugation (400 × *g*, 5 min, 4°C) and cell counts obtained using a Coulter Z2 particle counter (Beckman Coulter, Miami, FL).

Cell culture: Alveolar macrophages (AM) cells were suspended in RPMI media supplemented with 10% fetal bovine serum, 0.05 mM 2-mercaptoethanol, sodium pyruvate, and supplemented with an antimycotic/antibiotic cocktail (Mediatech, Manassas, VA). Cells were suspended at 1×10^6 cells per mL and then lipopolysaccharide (LPS, Sigma, St Louis, MO) at 20 ng/mL was added as described above for THP-1 cells. A 100 μl sample (100,000 cells) of cells was exposed to each MWCNT (ex: high dose 50 μg/mL equivalent to 5 μg/10^5 cells equivalent to 15.62 μg/cm^2 (5 μg on .32 cm^2)) and experiments were conducted in 96-well plates for 24 h in 37°C water-jacketed CO_2 incubators (ThermoForma, Houston, TX). Particle concentrations tested were 0, 6.25, 12.5, 25, 50 μg/mL. Media was collected for IL-1β assay and cell viability was determined by MTS assay. Ten to 12 mouse lung lavage collections were pooled each time, and the experiment was replicated three to four times.

Bioactivity assays

MTS Assay: Cell viability was determined by MTS reagent using the CellTiter^{96} assay (Promega, Madison, WI), according to the manufacturer's protocol. This assay used a MTS

dye read by a colorimetric plate reader (Molecular Devices, Sunnyvale, CA). In order to avoid distortions in the optical density values, steps were taken to remove the MTS reagent (transferring it into another plate) from the cell/particle mixture adhered to the plate bottom. The formation of bubbles was avoided and the plate was read at 490 nm.

LDH assay: Lactate dehydrogenase (LDH) was determined in 24 h culture supernatants by using CellTox^{96} assay (Promega, Madison, WI) according to the manufacturer's protocol. Data were expressed as % LDH relative to 100% cell death (obtained from lysed cells just prior to assay).

Cytokine Assay: Mouse IL-1β DuoSets were obtained from R&D Systems (R&D Systems, Minneapolis, MN) and ELISA assays performed according to the manufacturer's protocol.

Statistical Analyses

Statistical analyses involved comparison of means using a one- or two-way *ANOVA* followed by Holm-Sidak test to compensate for increased type I error. Statistical significance was the probability of type I error at less than 5% ($P < 0.05$). The minimum number of experimental replications was 3. Graphics and analyses were performed on PRISM v.7.0 and SPSS v.22.0.

Results

Particle Characterization

SEM and TEM images of MWCNT-COOH, Ag-MWCNT-COOH, GO and Ag-GO are shown in Figure 1. There was minimum change in structure after carboxylation or metal deposition. Silver particles on the nanotube and GO surface were seen as bright spots in SEM images and black spots in TEM images. This showed uniformity in metal nanoparticles deposition on MWCNT and GO. The elemental analysis by EDX confirmed the presence of Ag particles on the surface of CNTs and GO to be 29 and 19% respectively. TGA was used to quantify the metal nanoparticle loading in the hybrid materials. As shown in Figure 2 the resulting weight above 600° C was attributed to the weight of residual nano-metal, which is consistent with EDX data.

Particle toxicity/bioactivity in the C57BL/6 alveolar macrophage *in vitro* model

Figure 3A shows the relative cell death of AM isolated from C57BL/6 mice following a 24-hour culture. All of the particle derivations produced some measurable cell death with increasing concentrations, but the Ag-GO stood out as a particularly toxic particle. The small percentage of Ag on the Ag-GO particle could not account for the toxicity alone, so this was indicative of an interaction with the GO as tested in this cell model. In contrast, Figure 3B shows no apparent correlation between toxicity and resulting IL-1β release (NLRP3 inflammasome activation) of the Ag nanospheres or Ag composites. Only the source MWCNT and source GO showed any significant activation of the NLRP3 inflammasome and resulting IL-1β release.

Particle toxicity/bioactivity in the transformed THP-1 macrophage *in vitro* model

Figure 4A shows the relative cell death of THP-1 cells following a 24-hour culture. All of the particle derivations produced some measurable cell death at the highest concentration. In contrast, to the C57BL/6 AM model, Ag was not nearly as toxic and there was no isolated sensitivity to the Ag-GO variant. Figure 4B shows IL-1β release as a surrogate marker of NLRP3 inflammasome activation associated with MWCNT, carboxylated MWCNT and Ag nanospheres. The Ag composite materials showed no increase in IL-1β.

Toxicity in both cell models primarily due to Ag

Only 29% of the total mass of the Ag-MWCNT-COOH consisted of Ag. We, therefore, examined the relative toxicity in the two exposure models to low concentration Ag corresponding to the amount on the MWCNT to determine the probability that the combined particle toxicity was due to the Ag alone or to the addition of the Ag to the MWCNT. Figure 5 shows the results of toxicity for Ag nanospheres at low concentrations using two different assays. Figure 5A shows a linear trend of increasing toxicity (by LDH assay) in the C57BL/6 AM, but is in contrast to the MTS assay result in Figure 5B, which shows very little toxicity over the selected concentration range. Figures 5C and 5D, the analogous data for the THP-1 model, is more consistent as there is no increase in toxicity for the LDH assay and a slight proliferation indicated by the MTS assay. The MTS assay can detect both toxicity and proliferation while the LDH assay only detects cell death so the results in Figures 5C and 5D are not contradictory. This slight proliferation is apparent in Figure 4A also (blue line) at the lowest concentrations of the Ag nanospheres. It has been previously suggested that the MTS assay, done correctly, is superior to the LDH assay in particle-exposure studies (Xia et al. 2013). If the MTS result is used to determine that the low Ag concentrations do not induce a toxic response in either model, it may be concluded that any toxicity resulting from the Ag-carbon particles is a result of the interaction of the two materials as the carbon component does not account for all the toxicity either.

Figure 6 breaks this distinction down further by showing the toxicity as a fraction of toxicity induced by the Ag content for both cell models and for both carbon particles (COOH-MWCNT and its Ag derivative and GO and its Ag derivative) contrasted with pure Ag nanospheres. Only the highest concentrations of particle in the C57BL/6 AM model show a slight contribution of Ag to the overall toxicity. The THP-1 cell model does not have any contribution of Ag to the toxicity of the metal-doped carbon particles. This further shows the differences in the two models and their response to silver.

Silver Ion Release in Ag Cell Culture Media

The silver ion concentration released from Ag-MWCNT-COOH, Ag-GO and Ag nanospheres in ALF were measured by ICP-MS (Table 1). The amount of silver ions released from Ag-MWCNT-COOH and Ag-GO was similar and much lower than that of Ag nanospheres, which was consistent with toxicity result for the primary AM seen in Figure 4. There was no difference in terms of particle size among the three samples, which indicated that the particle size did not affect the toxicity.

Discussion

Carbon nanotubes (MWCNT) and graphene oxide (GO) have attracted much attention due to their specific morphological, mechanical, and electrical properties. The large specific surface area make CNT good supporting materials for the deposition of metals such as Ag, Au, Pt, Pd, which are used in catalysts, fuel cells, biosensors, spectroscopic probes, surface-enhanced Raman scattering substrates, semiconductors, and optoelectronic devices (Chin et al. 2005; Pasricha et al. 2009; Xu and Wang 2009; Shen et al. 2010). It is generally assumed that the adsorption between silver and carbon material will prevent the silver ions release from particles to some degree, reducing the toxicity. First, there are oxygen containing functional groups on the surface of oxidized MWCNT and GO. The negatively charged surface can attract silver ions to prevent them from being released in the media. The electron clouds on the surface of carbon nanotubes provide a mild attractive force between the nanotubes as well as Ag^+ (Booker and Boysen 2011). Secondly, some reductants may reverse the ion release reaction. These include groups containing C=C, and hydroxyl groups, as well as oxidation debris that are known to have structures similar to organic acids (Liu J and Hurt RH 2010; Stéfani et al. 2011). Finally, carboxyl groups on functionalized MWCNT and GO exist in the form of COO^-in aqueous media, which serve as a buffer and hydrolyze with H^+ to form COOH, resulting in a lower H^+ concentration and hence inhibiting the silver oxidation reaction (Equation 1). It is likely that the toxicity of silver composites depends not only on their existing forms, but also surface functionalization, temperature and media. In the present study the toxicity of silver-carbon material composites in addition to silver nanospheres was evaluated to test this assumption. The objective of this research was to determine if coating silver on MWCNT and GO could reduce the toxicity of silver.

The findings in this study suggest that specific outcomes may well depend on the model under examination. For example, marked differences in effects of toxicity of Ag nanospheres have been previously shown using three epithelial cell lines, in addition to MARCO null C57BL/6 AM (Hamilton et al. 2014). In this study two different cell models were selected based on previous experience and relevance. The most likely relevant model would be the primary AM from mice. The reasons for this decision are that they are normal primary cells and are being used soon after isolation and without modification. They are highly phagocytic cells that rapidly accumulate nanomaterials *in vivo* (Nakayama 2018). While THP-1 cells have been used to examine toxicity and cellular effects of nanomaterials, they are an acute monocytic leukemia cell line, that have to be modified into being macrophage-like and are not equally phagocytic for all materials. For example, we have noted relatively poor response to crystalline silica particles by THP-1 cells compared to primary alveolar macrophages (Xia et al. 2013). A key aspect of the toxicity of Ag appears to be the dissociation of Ag ions that has been previously shown to be proportional to the surface area (Hamilton et al. 2014). The dissociation would be accelerated in the acidic conditions of the phagolysosome. What is not certain is whether there may be differences in the pH between the phagolysosomes of primary alveolar macrophages and those of differentiated THP-1 cells accounting for differences in the toxicity/bioactivity data shown in Figures 3 and 4.

The model differences regarding toxicity and NLRP3 inflammasome activation could be the result of several factors. First, lytic cell death or rapid necrosis has been found to attenuate

the NLRP3 inflammasome activation (Martin-Sanchez et al. 2017). The results from this study suggest that the mouse AM model is simply more sensitive to the free Ag ions after the particles were internalized. The PMA treatment used with the THP-1 cells intentionally created an aggressively phagocytic, activated cell that did not process particles in a normal manner. In contrast, the primary mouse AM was not activated and intracellular trafficked the particles at a normal pace. This could have resulted in a more efficient release of Ag ions, particularly in the acidic compartments of the phagolysosome. In addition, another possibility is the lack of a second signal in the THP-1 model interfering with the NF-kB activation/timing required for NLRP3 inflammasome activation. Lastly, there have been recently discovered inhibitors of the NLRP3 inflammasome, and these may simply be more prevalent in the THP-1 model (Song et al. 2016; Malireddi et al. 2018). Further experiments would need to be conducted to determine the precise difference between cell models.

In summary, both Ag-MWCNT-COOH and Ag-GO had lower toxicity than Ag nanospheres based on Ag content. Therefore, the content of Ag in the silver composites does not appear to contribute to their toxicity or explain the increased toxicity of Ag-GO in murine AM. The primary reason for this appears to be the decreased rate of Ag ion release from particles even under the acidic conditions of phagolysosomes. Finally, murine AM may represent a more sensitive model for *in vitro* testing suggesting that reliance solely on macrophage cell lines may provide misleading results.

Acknowledgments

Funding

All work was supported by NIH Research Grant, R01 ES023209 and CoBRE Grant, P30 GM10338.

References:

Abou El-Nour KMM, Eftaiha Aa, Al-Warthan A, Ammar RAA. 2010 Synthesis and applications of silver nanoparticles. Arabian Journal of Chemistry. 3(3):135–140.

Booker RD, Boysen E. 2011 Nanotechnology for dummies. John Wiley & Sons.

Bouwmeester H, Poortman J, Peters RJ, Wijma E, Kramer E, Makama S, Puspitaninganindita K, Marvin HJ, Peijnenburg AA, Hendriksen PJ. 2011 Characterization of translocation of silver nanoparticles and effects on whole-genome gene expression using an in vitro intestinal epithelium coculture model. ACS nano. 5(5):4091–4103. [PubMed: 21480625]

Chang Y-N, Zhang M, Xia L, Zhang J, Xing G. 2012 The toxic effects and mechanisms of CuO and ZnO nanoparticles. Materials. 5(12):2850–2871.

Chen Y, Mitra S. 2008 Fast Microwave-Assisted Purification, Functionalization and Dispersion of Multi-Walled Carbon Nanotubes. Journal of Nanoscience and Nanotechnology. 8(11):5770–5775. [PubMed: 19198303]

Chin KC, Gohel A, Chen WZ, Elim HI, Ji W, Chong GL, Sow CH, Wee ATS. 2005 Gold and silver coated carbon nanotubes: An improved broad-band optical limiter. Chemical Physics Letters. 409(1–3):85–88.

Choi O, Hu Z. 2008 Size dependent and reactive oxygen species related nanosilver toxicity to nitrifying bacteria. Environmental science & technology. 42(12):4583–4588. [PubMed: 18605590]

Chudasama B, Vala AK, Andhariya N, Upadhyay R, Mehta R. 2009 Enhanced antibacterial activity of bifunctional Fe3O4-Ag core-shell nanostructures. Nano Research. 2(12):955–965.

Dostert C, Petrilli V, Van Bruggen R, Steele C, Mossman BT, Tschopp J. 2008 Innate immune activation through Nalp3 inflammasome sensing of asbestos and silica [Research Support, N.I.H.,

Extramural Research Support, Non-U.S. Gov't]. Science. 320(5876):674–677. eng. [PubMed: 18403674]

Guo J-Z, Cui H, Zhou W, Wang W. 2008 Ag nanoparticle-catalyzed chemiluminescent reaction between luminol and hydrogen peroxide. Journal of Photochemistry and Photobiology A: Chemistry. 193(2–3):89–96.

Hadrup N, Lam HR. 2014 Oral toxicity of silver ions, silver nanoparticles and colloidal silver – A review. Regulatory Toxicology and Pharmacology. 68(1):1–7. [PubMed: 24231525]

Hamilton RF, Buckingham S, Holian A. 2014 The effect of size on Ag nanosphere toxicity in macrophage cell models and lung epithelial cell lines is dependent on particle dissolution. International journal of molecular sciences. 15(4):6815–6830. [PubMed: 24758926]

He D, Ikeda-Ohno A, Boland DD, Waite TD. 2013 Synthesis and Characterization of Antibacterial Silver Nanoparticle-Impregnated Rice Husks and Rice Husk Ash. Environmental Science & Technology. 47(10):5276–5284. [PubMed: 23614704]

Hussain SM, Schlager JJ. 2009 Safety Evaluation of Silver Nanoparticles: Inhalation Model for Chronic Exposure. Toxicological Sciences. 108(2):223–224. [PubMed: 19237550]

Kim YH, Lee DK, Cha HG, Kim CW, Kang YS. 2007 Synthesis and characterization of antibacterial Ag-SiO2 nanocomposite. The Journal of Physical Chemistry C. 111(9):3629–3635.

Kittler S, Greulich C, Diendorf J, Koller M, Epple M. 2010 Toxicity of Silver Nanoparticles Increases during Storage Because of Slow Dissolution under Release of Silver Ions. Chem Mater. 22(16): 4548–4554. English.

Lee D, Cohen RE, Rubner MF. 2005 Antibacterial properties of Ag nanoparticle loaded multilayers and formation of magnetically directed antibacterial microparticles. Langmuir. 21(21):9651–9659. [PubMed: 16207049]

Liu J, Hurt RH. 2010 Ion Release Kinetics and Particle Persistence in Aqueous Nano-Silver Colloids. Environmental Science & Technology. 44(6):2169–2175. [PubMed: 20175529]

Liu J, Sonshine DA, Shervani S, Hurt RH. 2010 Controlled Release of Biologically Active Silver from Nanosilver Surfaces. ACS Nano. 4(11):6903–6913. [PubMed: 20968290]

Liu JY, Hurt RH. 2010 Ion Release Kinetics and Particle Persistence in Aqueous Nano-Silver Colloids. Environmental science & technology. 44(6):2169–2175. English. [PubMed: 20175529]

Liu P, Zhao M. 2009 Silver nanoparticle supported on halloysite nanotubes catalyzed reduction of 4-nitrophenol (4-NP). Applied Surface Science. 255(7):3989–3993.

Malireddi RKS, Gurung P, Mavuluri J, Dasari TK, Klco JM, Chi H, Kanneganti TD. 2018 TAK1 restricts spontaneous NLRP3 activation and cell death to control myeloid proliferation. J Exp Med. 215(4):1023–1034. [PubMed: 29500178]

Manno D, Filippo E, Di Giulio M, Serra A. 2008 Synthesis and characterization of starch-stabilized Ag nanostructures for sensors applications. Journal of Non-Crystalline Solids. 354(52–54):5515–5520.

Marques MRC, Loebenberg R, Almukainzi M. 2011 Simulated Biological Fluids with Possible Application in Dissolution Testing. Dissolut Technol. 18(3):15–28. English.

Martin CR, Preedy VR, Hunter RJ. 2012 Nanomedicine and the Nervous System. CRC Press.

Martin-Sanchez F, Martinez-Garcia JJ, Munoz-Garcia M, Martinez-Villanueva M, Noguera-Velasco JA, Andreu D, Rivas L, Pelegrin P. 2017 Lytic cell death induced by melittin bypasses pyroptosis but induces NLRP3 inflammasome activation and IL-1beta release. Cell death & disease. 8(8):e2984. [PubMed: 28796264]

Maurer-Jones MA, Mousavi MPS, Chen LD, Buhlmann P, Haynes CL. 2013 Characterization of silver ion dissolution from silver nanoparticles using fluorous-phase ion-selective electrodes and assessment of resultant toxicity to Shewanella oneidensis [10.1039/C3SC50320H]. Chemical Science. 4(6):2564–2572.

Morones JR, Elechiguerra JL, Camacho A, Holt K, Kouri JB, Ramírez JT, Yacaman MJ. 2005 The bactericidal effect of silver nanoparticles. Nanotechnology. 16(10):2346. [PubMed: 20818017]

Nakayama M 2018 Macrophage Recognition of Crystals and Nanoparticles [Review]. Frontiers in Immunology. 9(103). English.

Palomaki J, Valimaki E, Sund J, Vippola M, Clausen PA, Jensen KA, Savolainen K, Matikainen S, Alenius H. 2011 Long, needle-like carbon nanotubes and asbestos activate the NLRP3

inflammasome through a similar mechanism [Research Support, Non-U.S. Gov't]. ACS Nano. 5(9):6861–6870. eng. [PubMed: 21800904]

Pasricha R, Gupta S, Srivastava AK. 2009 A Facile and Novel Synthesis of Ag–Graphene-Based Nanocomposites. Small. 5(20):2253–2259. [PubMed: 19582730]

Porter D, Sriram K, Wolfarth M, Jefferson A, Schwegler-Berry D, Andrew ME, Castranova V. 2008 A biocompatible medium for nanoparticle dispersion. Nanotoxicology. 2(3):144–154.

Rashid MU, Bhuiyan MKH, Quayum ME. 2013 Synthesis of silver nano particles (Ag-NPs) and their uses for quantitative analysis of vitamin C tablets. Dhaka University Journal of Pharmaceutical Sciences. 12(1):29–33.

Shen J, Shi M, Li N, Yan B, Ma H, Hu Y, Ye M. 2010 Facile synthesis and application of Ag-chemically converted graphene nanocomposite. Nano Research. 3(5):339–349. English.

Song H, Liu B, Huai W, Yu Z, Wang W, Zhao J, Han L, Jiang G, Zhang L, Gao C et al. 2016 The E3 ubiquitin ligase TRIM31 attenuates NLRP3 inflammasome activation by promoting proteasomal degradation of NLRP3. Nat Commun. 7:13727. [PubMed: 27929086]

Stéfani D, Paula AJ, Vaz BG, Silva RA, Andrade NF, Justo GZ, Ferreira CV, Filho AGS, Eberlin MN, Alves OL. 2011 Structural and proactive safety aspects of oxidation debris from multiwalled carbon nanotubes. Journal of Hazardous Materials. 189(1–2):391–396. [PubMed: 21429665]

Xia T, Hamilton RF, Bonner JC, Crandall ED, Elder A, Fazlollahi F, Girtsman TA, Kim K, Mitra S, Ntim SA et al. 2013 Interlaboratory evaluation of in vitro cytotoxicity and inflammatory responses to engineered nanomaterials: the NIEHS Nano GO Consortium [Research Support, N.I.H., Extramural]. Environ Health Perspect. 121(6):683–690. eng. [PubMed: 23649538]

Xu C, Wang X. 2009 Fabrication of Flexible Metal-Nanoparticle Films Using Graphene Oxide Sheets as Substrates. Small. 5(19):2212–2217. [PubMed: 19662647]

Zhang L, Yu JC, Yip HY, Li Q, Kwong KW, Xu A-W, Wong PK. 2003 Ambient light reduction strategy to synthesize silver nanoparticles and silver-coated TiO2 with enhanced photocatalytic and bactericidal activities. Langmuir. 19(24):10372–10380.

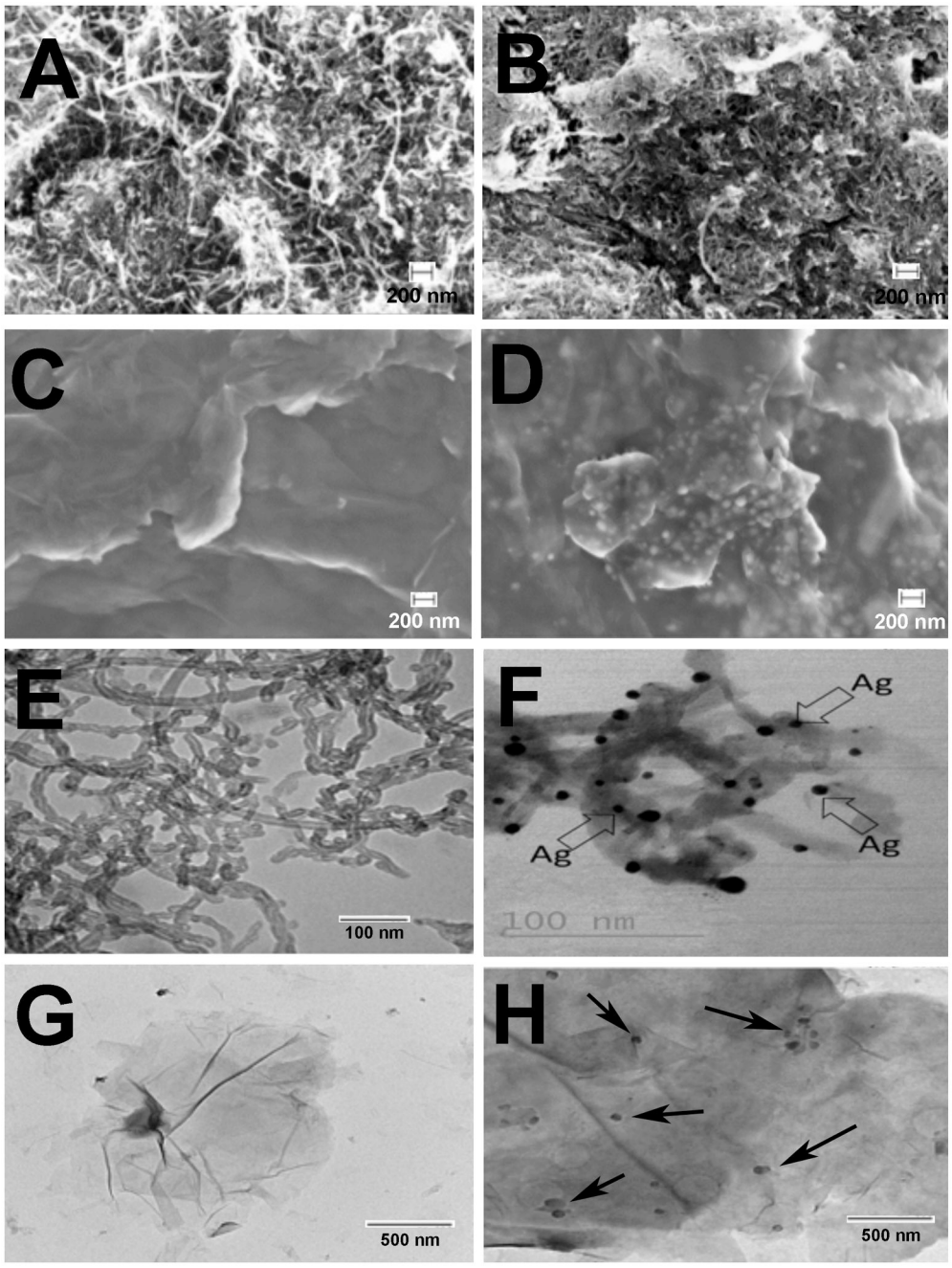

Figure 1:
SEM images of **A**) MWCNT-COOH, **B**) Ag-MWCNT-COOH, **C**) GO, **D**) Ag-GO TEM images of **E**) MWCNT-COOH, **F**) Ag-MWCNT-COOH, **G**) GO, **H**) Ag-GO. Arrows in panels F and H indicate Ag particle deposition on the carbon.

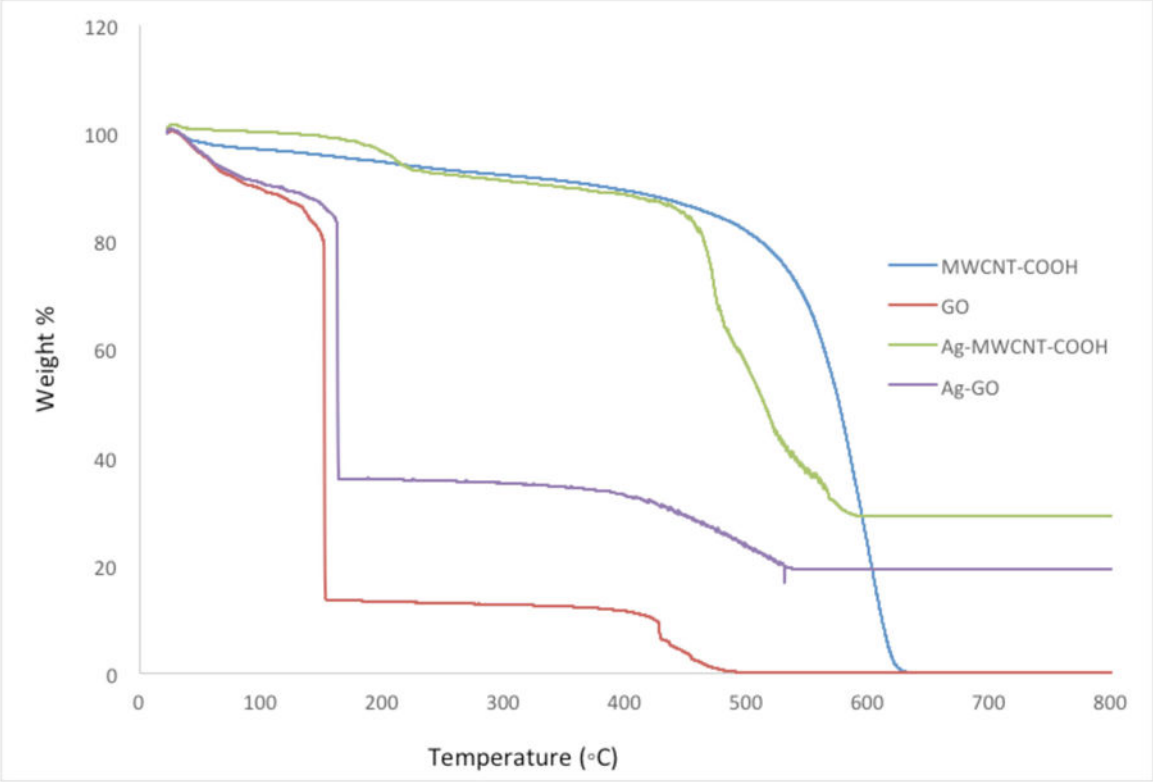

Figure 2:
Thermo Gravimetric Analysis (TGA) data for MWCNT, Ag-MWCNT-COOH, GO and Ag-GO. Data expressed as percent mass relative to increasing temperature up to 800° C.

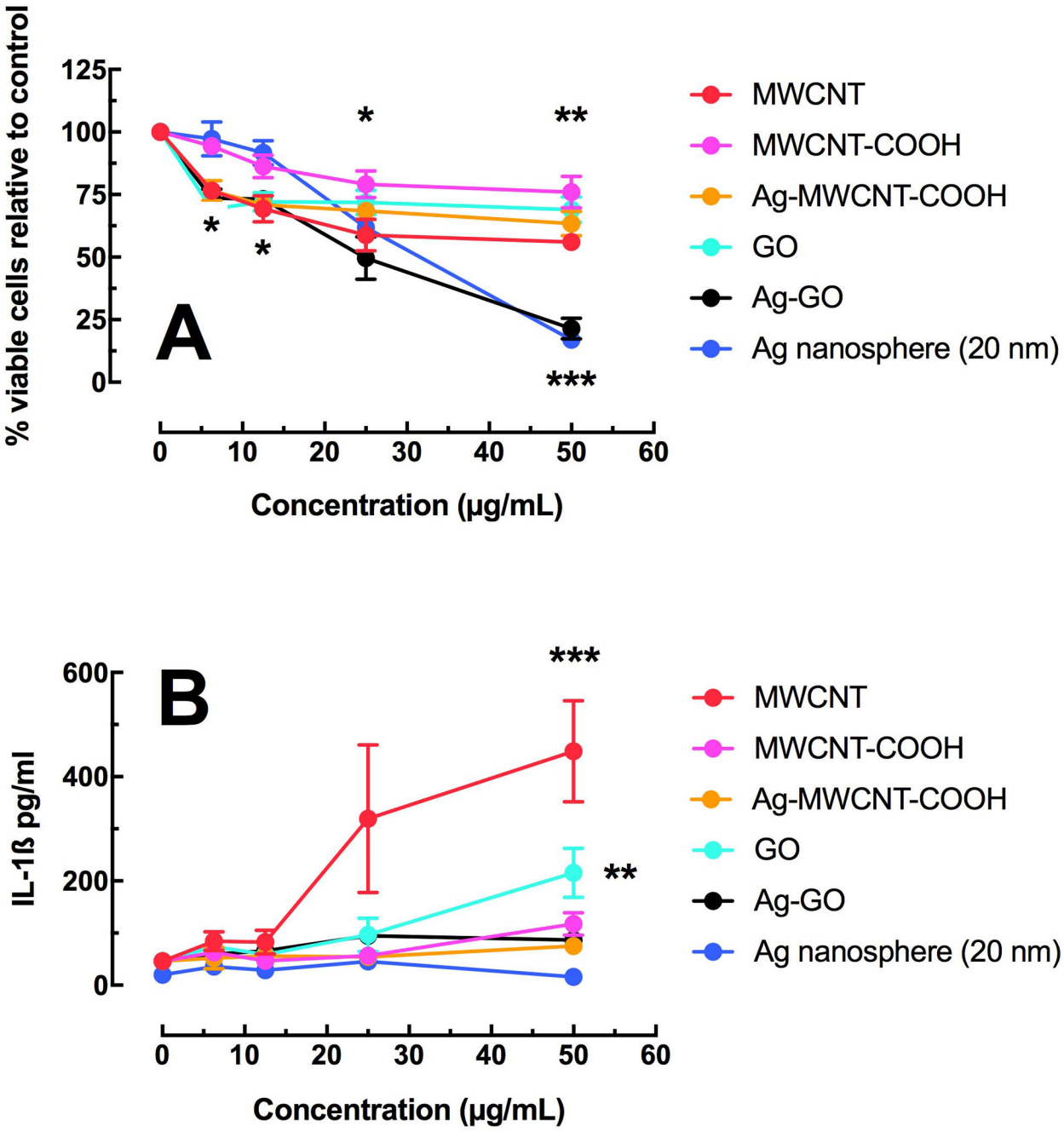

Figure 3:

Relative toxicity and bioactivity in the C57BL/6 alveolar macrophage model. **A**) Mean ± *SEM* cell viability by MTS assay after 24 hours of particle exposure. **B**) Mean ± *SEM* IL-1β release after 24 hours of particle exposure with LPS co-culture. Asterisks *** indicate $P < 0.001$, ** $P < 0.01$ or * $P < 0.05$ compared to 0 µg/mL control condition.

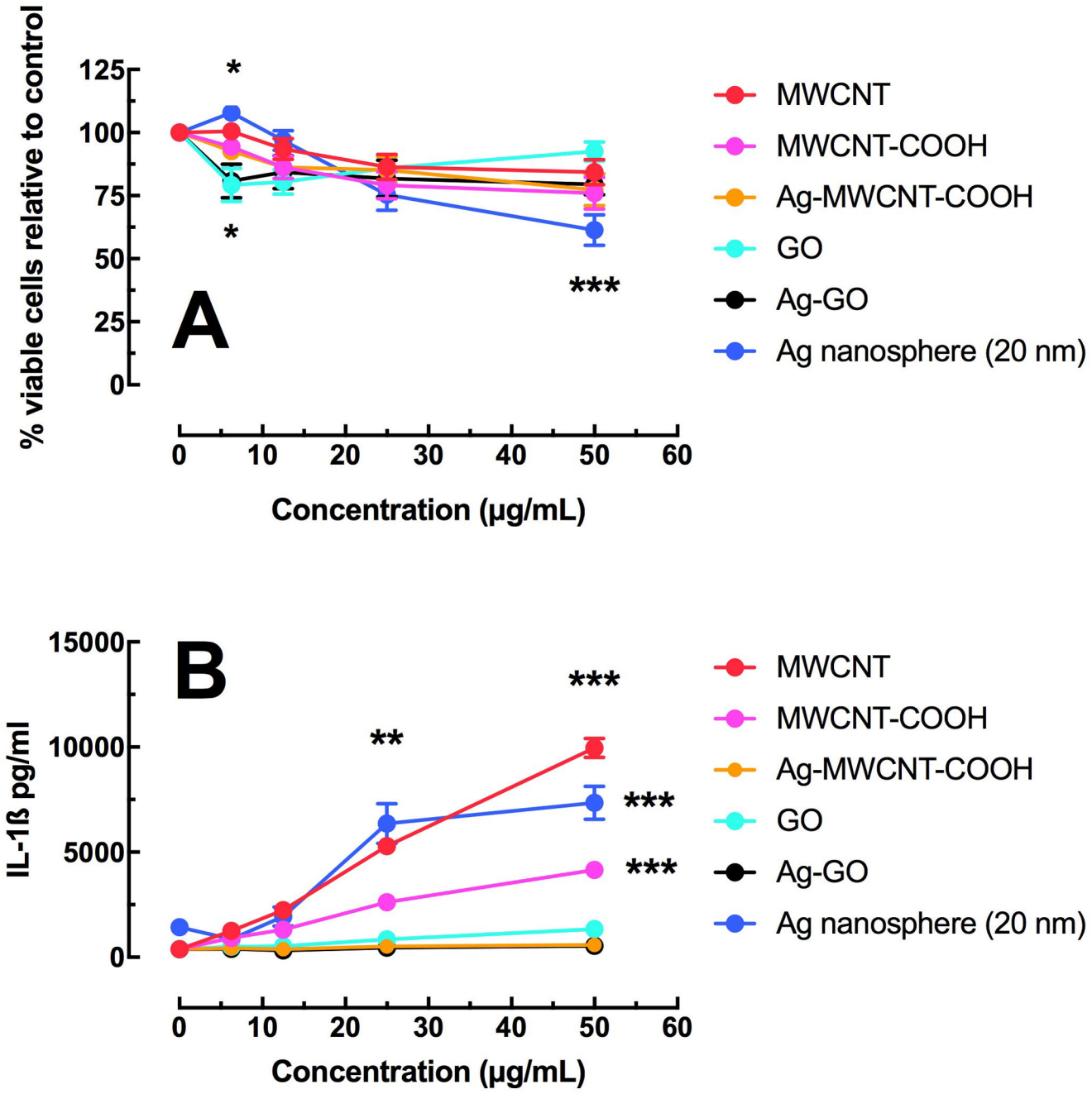

Figure 4:

Relative toxicity and bioactivity in the transformed THP-1 macrophage model. **A**) Mean ± *SEM* cell viability by MTS assay after 24 hours of particle exposure. **B**) Mean ± *SEM* IL-1β release after 24 hours of particle exposure with LPS co-culture. Asterisks *** indicate $P < 0.001$, ** $P < 0.01$ or * $P < 0.05$ compared to 0 µg/mL control condition.

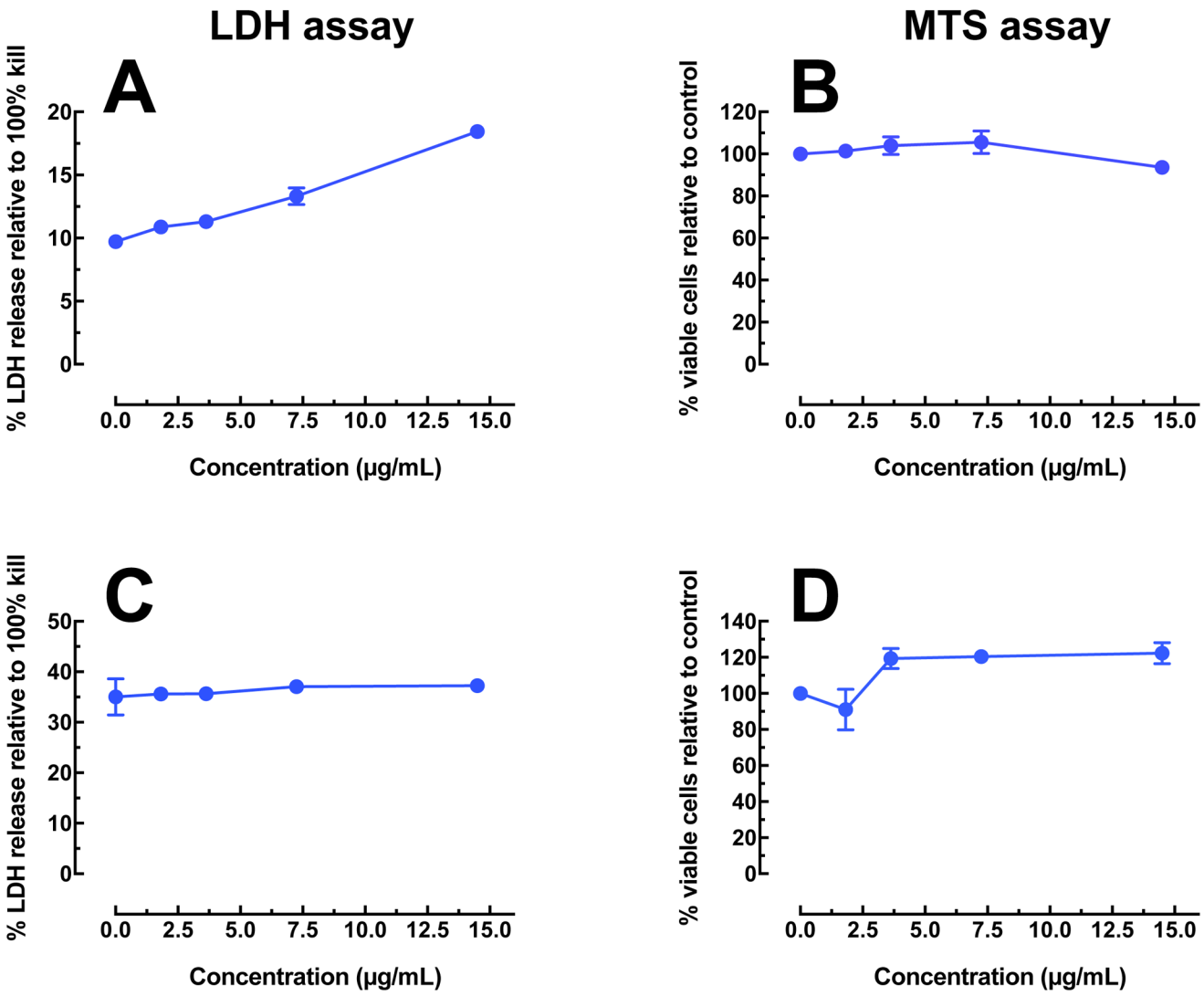

Figure 5:

Toxicity of Ag nanosphere (20 nm) at low concentrations, representing relative amounts corresponding to the MWCNT (12.5 to 50 μg/mL), by two different assays. **A**) Toxicity in C57BL/6 alveolar macrophages by LDH assay. **B**) Toxicity/proliferation in C57BL/6 alveolar macrophages by MTS assay. **C**) Toxicity in THP-1 cells by LDH assay. **D**) Toxicity/proliferation in THP-1 cells by MTS assay.

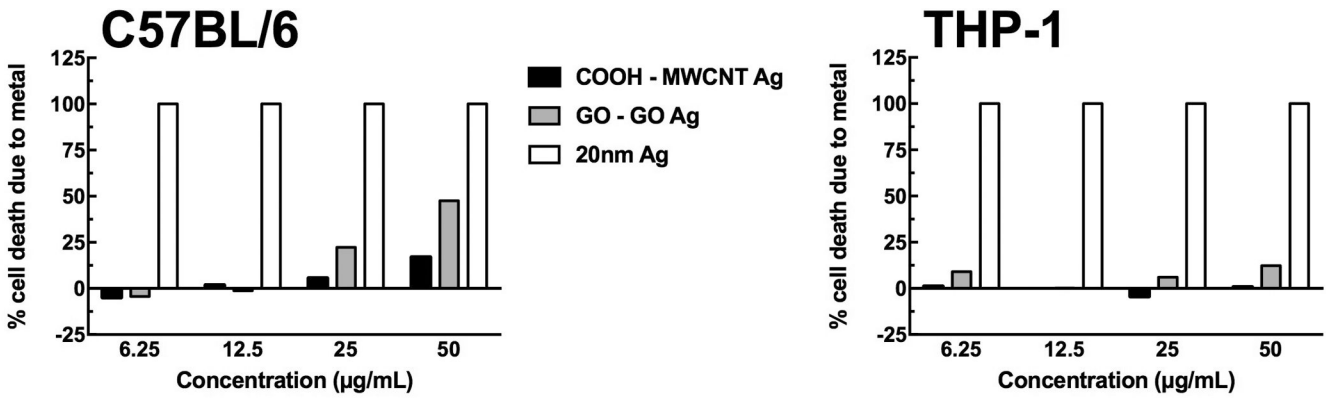

Figure 6:

Relative cell death caused by the metal (Ag) content of the MWCNT in C57BL/6 alveolar macrophages and THP-1 cells in 24 hr *in vitro* particle exposures. Data was extrapolated from the dose-response data presented earlier factored with the Ag content of the MWCNT variants.

Table 1:

Particle size and Ag ion concentration from ICP-MS of silver solutions.

Particle suspension/solutions	Particle size (nm)	Ag^+ (ppb)
Ag-MWCNT-COOH	1.2 ± 0.3	20
Ag-GO	1.8 ± 0.2	24
Ag	1.0 ± 0.1	92

Table 2:

Particle characterization. Agglomerate size and zeta potential in RPMI culture media. Endotoxin measured from raw particles.

Particle	Size (Mean nm ± S.D.)	Zeta Potential (Mean mV ± S.D.)	Endotoxin U/mL and ng/mL*	
MWCNT	332.3 ± 132.2	−12.06 ± 0.666	9.3	0.93
Ag-MWCNT-COOH	210.7 ± 544.5	−10.24 ± 1.29	43	4.3
MWCNT-COOH	126.3 ± 9.8	−11.23 ± 0.4	41	4.1
GO	169.3 ± 46.6	−10.36 ± 1.27	27	2.7
Ag-GO	217.7 ± 5.7	−10.29 ± 0.47	42	4.2

* Unit conversion approximately 1U equal to 0.1ng.